Geochimica et Cosmochimica Acta, Vol. 68, No. 24, pp. 5071–5079, 2004

0016-7037/04 $30.00 + .00

doi:10.1016/j.gca.2004.05.048

Al environment in tectosilicate and peraluminous glasses: A ^{27}Al MQ-MAS NMR, Raman, and XANES investigation

DANIEL R. NEUVILLE,[1,*] LAURENT CORMIER,[2] and DOMINIQUE MASSIOT[3]

[1]Physique des Minéraux et des Magmas, CNRS-UMR7047, Institut de Physique du Globe de Paris, 4 place Jussieu 75005 Paris, France
[2]Laboratoire de Minéralogie-Cristallographie, Universités Paris 6 et 7, CNRS UMR 7590, Institut de Physique du Globe de Paris, 4 place Jussieu, 75005 Paris, France
[3]CRMHT-CNRS, 1D av. Recherche Scientifique, 45071 Orléans cedex 2, France

(*Received January* 21, 2004; *accepted in revised form May* 11, 2004)

Abstract—Tecto-aluminosilicate and peraluminous glasses have been prepared by conventional and laser heating techniques, respectively, in the CaO-Al_2O_3-SiO_2 system. The structure of these glasses were studied using Raman spectroscopy, X-ray absorption at the Al K-edge and ^{27}Al NMR spectroscopy with two different high fields (400 and 750 MHz). Raman spectroscopy and X-ray absorption are techniques sensitive to the network polymerization and, in particular, show different signal as a function of silica content. However, these two techniques are less sensitive than NMR to describe the local aluminium environment. For tectosilicate glasses, aluminium in five-fold coordination, $^{[5]}$Al, was found and a careful quantification allows the determination of a significant amount of $^{[5]}$Al (7% in the anorthite glass). The proportion of $^{[5]}$Al increases for the peraluminous glasses with small amounts (<2%) of six-fold coordination, $^{[6]}$Al. The presence of $^{[5]}$Al agrees with previous observations of the existence of nonbridging oxygens (NBOs) in tectosilicate compositions. However, the proportion of $^{[5]}$Al in the present study indicates that no major proportion of triclusters (oxygen coordinated to three (Si,Al)O_4 tetrahedra) is required to explain these NBOS. *Copyright © 2004 Elsevier Ltd*

1. INTRODUCTION

Understanding the structure of calcium aluminosilicate glasses is of great interest for technological or geological applications. These glasses are attractive materials due to their highly refractory nature and their excellent optical and mechanical properties (Lines et al., 1989; Wallenberger and Brown, 1994). They also can be considered as frozen approximation of melts, for which a detailed knowledge of the structure is needed to better constrain the modeling of magmatic processes. Some glasses in this ternary system are also good candidate for the storage of waste (Neuville et al., 2003). The CaO-Al_2O_3-SiO_2 (CAS) system is remarkable because glasses from pure SiO_2 to calcium aluminate can be synthesized using normal quench rate (10°/s), contrary to alkali or Mg aluminosilicate glasses.

Aluminum plays different roles as a function of the CaO/Al_2O_3 ratio. When CaO/Al_2O_3 > 1, Al is in tetrahedral position. Recently, several experimental and theoretical studies (Cormier et al., 2000, 2003, 2004; Neuville et al., 2004) have related the Al speciation and glass transition variations for low-silica CAS glasses. At high CaO content, Al was found in depolymerized species such as Q^2 and Q^3 (Q^n corresponds to tetrahedral site, SiO_4 or AlO_4, where *n* is the number of bridging oxygens per tetrahedron) in calcium aluminate glasses. With increasing content of SiO_2 and/or Al_2O_3, Al is found preferentially in Q^4 sites while Si is distributed in all Q^n species. The proportion of Al in Q^2 and Q^3 species decreases rapidly with increasing SiO_2 or Al_2O_3 which implies a rapid increase of the glass transition temperature for the low silica glasses. This is confirmed by a ^{17}O NMR study that indicates a strong preference for non bridging oxygens (NBOs) to be localized on Si (Allwardt et al., 2003).

It is usually assumed that two AlO_4 tetrahedra must be associated with one calcium ion to ensure charge compensation. Along the tectosilicate join (CaO/Al_2O_3 = 1), the role of Ca is purely charge compensating and previous structural studies have shown that Al is present in tetrahedral sites (Mysen et al., 1981, 1982; Seifert et al., 1985). According to composition, tectosilicate glasses have no NBOs and must consist of fully polymerized (Si,Al)O_4 tetrahedral units forming a three-dimensional network structure (Mysen, 1988). Raman spectroscopy results suggest two structural units which differ in T-O-T angle (Seifert et al., 1982) (with T = Si, Al) and X-ray diffraction data indicate that anorthite glass contains four-membered rings (Taylor and Brown, 1979). Molecular Dynamics (MD) simulations are also consistent with the presence of such small rings in the Al_2O_3 rich glasses (Cormier et al., 2003). The concept of fully polymerized glasses for tectosilicate glasses has been recently reassessed with the ^{17}O NMR evidence for excess NBOs in an anorthite glass (Stebbins and Xu, 1997). To explain these NBOs and viscosity variations, it has been suggested that oxygen coordinated to three TO_4 tetrahedra, the so-called tricluster, could be an energetically stable complex in such compositions (Lacy, 1963; Toplis et al., 1997a). There has been extensive speculation about the existence of these triclusters since, up to now, no direct evidence for their presence has been detected experimentally though they are present in MD simulations of CAS glasses (Benoit et al., 2001; Cormier et al., 2003). Another model proposed the presence of five ($^{[5]}$Al) or six ($^{[6]}$Al) fold coordinated species in peraluminous glasses (Mysen et al., 1981). Evidence of $^{[5]}$Al has been recently reported in an anorthite glass (Stebbins et al., 2000) though the estimated proportion (1 ± 0.5%) is not sufficient to explain the

* Author to whom correspondence should be addressed (neuville@ipgp.jussieu.fr).

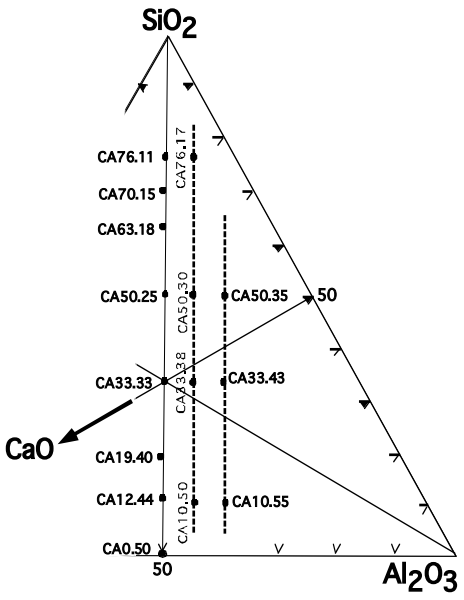

Fig. 1. Ternary CaO-Al_2O_3-SiO_2 system with the glass compositions studied (mol%).

number of NBOs detected in this glass (5 ± 1%) (Stebbins and Xu, 1997). In peraluminous composition ($CaO/Al_2O_3 < 1$), the local charge balance of the AlO_4 tetrahedra is no longer attained because not enough calcium atoms are present for charge-balance and Al may be in higher coordinated species. The presence and quantification of $^{[5]}Al$ and $^{[6]}Al$ has not yet been examined for these Al_2O_3-rich CAS compositions though such species may be formed simultaneously with NBOs, which should strongly affect the physical properties of the melt such as density, viscosity, compressibility, heat of mixing (Toplis et al., 1997b).

This paper is focused on peraluminous and tectosilicate glasses to understand better the structure of calcium aluminosilicate glasses and in particular the role of Al^{3+}. Raman spectroscopy, X-ray absorption spectroscopy (XAS) at the Al K-edge, and ^{27}Al NMR spectroscopy have been used. ^{27}Al NMR was applied to study the local environment of Al in the CAS glasses. A quantitative determination of the proportion of $^{[5]}Al$ was determined which indicates higher proportion of $^{[5]}Al$ in tectosilicate glasses than previously estimated. Little amounts of $^{[6]}Al$ sites have been detected in peraluminous compositions. These Al coordination change is also affecting the Raman and XANES spectra. All three approaches provide a better knowledge of the Al environment near the tectosilicate compositions that should improve the understanding of the physicochemical properties of the aluminosilicate melts.

2. EXPERIMENTAL METHOD

2.1. Starting Materials

Tectosilicate glasses ($CaO/Al_2O_3 = 1$) were prepared by melting the appropriate quantities of Al_2O_3, $CaCO_3$ and SiO_2. We mixed ~100 g $CaCO_3$-Al_2O_3-SiO_2 (Rectapur from Merck) for 1 h under alcohol in an agate mortar. The mixture was heated slowly to decompose the carbonate and then heated up to 1900 K in covered Pt-alloy crucibles for a few hours in equilibrium with air. The sample was quenched in few seconds from high temperature by dipping the bottom of the platinum crucible into distilled water. The viscosity, transition temperatures and the thermodynamic parameters are given elsewhere (Neuville, 1992; Cormier et al., 2004). The chemical compositions are plotted in mol% in Figure 1 and given in Table 1.

Peraluminous glasses cannot be obtained by standard quenching techniques due to the high liquidus temperature. Sintered powders were melted in aerodynamic levitation device using air as a flowing gas and CO_2 laser as a heating source (CRMHT, Orléans) (Coté et al., 1992). The melting times are less than 1 min and the quench is obtained by switching off the power source. Clear glass beads with 1–5 mm in diameter were obtained. The quench rate is estimated to be ~200–300 Ks^{-1}. Chemical and glass homogeneity were checked by microprobe analysis and Raman spectroscopy. The chemical compositions of these glasses are given in Figure 1 and Table 1.

The glass density was measured using the Archimedes method with toluene as liquid reference (Table 1). The name of the glasses corresponds to the chemical composition CAx · y, with $x = SiO_2$, $y = Al_2O_3$ and $CaO = 100 - (x + y)$.

2.2. Raman Spectroscopy

Unpolarized Raman spectra were measured on a T64000 Jobin-Yvon confocal micro-Raman spectrometer equipped with a CCD detector. The 514.532 nm line of a Coherent 70 Ar^+ laser operating at 2 W was used as the exciting source. The integration time was 300 s and all spectra were recorded between 20 and 1650 cm^{-1} and corrected for temperature and frequency dependent scattering intensity using a correction factor of the form proposed by Long (Long, 1977) and given by Neuville and Mysen (1996). The corrected Raman intensities were normalized to the data point of the greatest absolute intensity. The spectra were deconvoluted using Igor software. In the curve-fitting procedure, wavenumbers, widths and intensities are independent and unconstrained variables.

2.3. XANES Spectroscopy

The X-ray absorption near-edge structure (XANES) spectra at the Al K-edge have been collected on the SA32 beamline at the SuperAco storage ring of LURE (Orsay, France), operating at 800 MeV and with a beam current in the range 100–300 mA. The beam was monochromatized using two α-quartz crystals cut along (10*1*0) with experimental resolution of 0.2 eV. X-ray absorption spectra were recorded in total electron yield detection mode in the photon energy range 1550–1650 eV with 0.2 eV steps and 1 s integration time. Three spectra were acquired and averaged for all samples. Further details of the acquisition conditions are given elsewhere (Neuville et al., 2004). All XANES spectra were calibrated with an Al metallic foil at the inflexion point of the K edge taken at 1559 eV and periodically checked. XANES spectra were normalized using XAFS software (Winterer, 1997). Second de-

Table 1. Chemical composition (in wt%)[a] and density of the glasses studied.

Sample	SiO_2	Al_2O_3	CaO	Density (g cm^3)
CA76.11	71.50 (2)	18.96 (5)	10.01 (3)	2.436 (4)
CA76.17	68.22 (6)	25.90 (8)	5.84 (5)	2.397 (7)
CA50.25	42.59 (8)	35.60 (7)	20.41 (8)	2.690 (6)
CA50.30	41.83 (4)	42.51 (9)	15.64 (4)	2.652 (5)
CA50.35	50.53 (7)	48.19 (7)	11.35 (7)	2.670 (9)
CA33.33	27.55 (7)	46.74 (5)	26.01 (3)	2.789 (7)
CA33.38	26.48 (6)	51.73 (7)	21.74 (9)	2.740 (8)
CA33.43	25.74 (8)	56.86 (6)	17.45 (6)	2.790 (6)
CA12.44	9.39 (9)	57.12 (1)	31.72 (4)	2.860 (3)
CA10.50	7.54 (6)	64.19 (6)	28.21 (5)	2.857 (9)
CA10.55	7.3 (4)	68.74 (7)	24.05 (8)	2.880 (7)

[a] Average of 16 analysis made with a Camebax electron microprobe at 15 kV and 10 nA with a 15-s counting time.

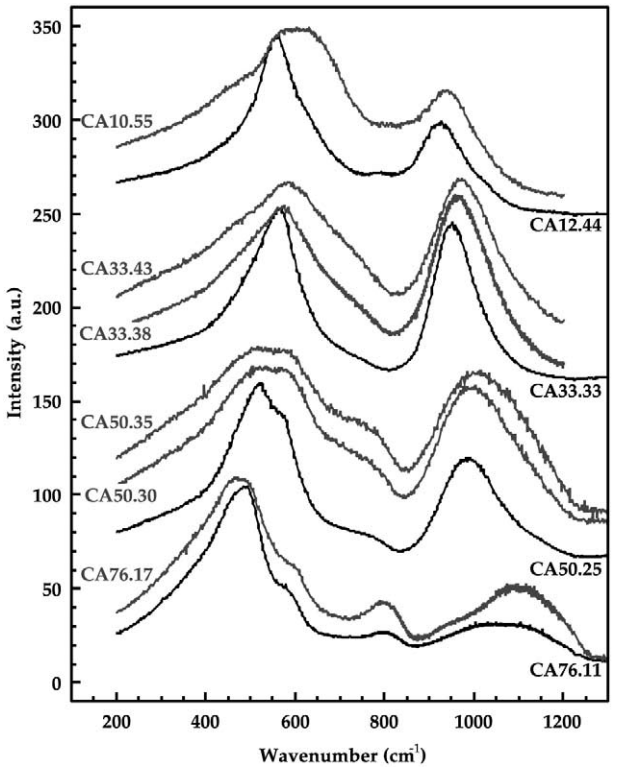

Fig. 2. Raman spectra for tectosilicate and peraluminous glasses.

rivatives of the XANES spectra were used to determine the position of the resonances.

2.4. High-Resolution Solid State NMR Spectroscopy

The high-resolution ^{27}Al NMR spectra have been obtained at two different principal fields (9.4 T—400 MHz and 17.6 T—750 MHz) on Bruker AVANCE instruments equipped with high speed MAS probeheads (spinning rates of 30 to 33 kHz, aluminum-free zirconia rotors of 2.5 mm diameter). The ^{27}Al one dimensional spectra have been acquired on large sweep width (2 MHz) with small pulse angle to ensure quantitative interpretation (Alemany et al., 1991). The Multiple Quantum Magic Angle Spinning (MQMAS) (Frydman et al., 1995; Medek et al., 1995; Frydman, 2002) experiments have been acquired using the shifted-echo pulse sequence with acquisition and processing of the full echo (Massiot et al., 1996) and synchronized acquisition of the indirect dimension (Massiot, 1996). The triple quantum excitation and conversion where achieved under high power irradiation (ν_{rf} ~150 kHz) and the shifted-echo generation with low power pulse (ν_{rf} ~12 kHz). For all samples, the measured spin-spin relaxation time, T_2, was checked to be long enough (>10 ms) to allow acquisition of the whole echo leading to pure phase 2D spectra with no rolling baseline.

3. RESULTS

3.1. Raman Spectroscopy

Raman spectra are plotted in Figure 2 for tectosilicate and peraluminous glasses. For discussion, we distinguished three regions in the Raman spectra: the low-frequency region (200–700 cm^{-1}), the midfrequency region (700–900 cm^{-1}) and the high-frequency region (900–1300 cm^{-1}).

3.1.1. Tectosilicate Glasses

3.1.1.1. Low-frequency region (200–700 cm^{-1}). The Raman spectra exhibit a strong band centered near 500 cm^{-1} for CA76.11 glass with a shoulder near 450 cm^{-1} and a tail to lower frequency. In addition, there is a band near 600 cm^{-1}. This spectrum is similar to other reported Raman spectra of silica-rich CAS glasses (McMillan et al., 1982; Seifert et al., 1982). For CA50.25, the band at 600 cm^{-1} is more intense and the one at 500 cm^{-1} is still present. These two bands merge in one narrow peak for glasses with lower SiO_2 content. The 600 cm^{-1} maximum peak becomes broader with decreasing SiO_2 content and shifts slowly towards lower frequency before completely disappearing at low SiO_2 content. A deconvolution of these bands is unsuccessful and they are associated with motions of bridged oxygen in T-O-T linkages. The band near 560 cm^{-1} in Al_2O_3-rich glasses is likely due to the presence of Al-O-Al bridges (McMillan et al., 1982; Seifert et al., 1982).

3.1.1.2. Midfrequency region (700–900 cm^{-1}). For CA76.11, a distinct peak at 800 cm^{-1} is observed. As the SiO_2 content decreases, the intensity decreases and this peak broadens and shifts to lower frequency. This peak disappears for composition with lower than 50% SiO_2. This band is usually ascribed to cage motion of Si-O stretching vibrations (McMillan et al., 1994).

3.1.1.3. High-frequency region (900–1300 cm^{-1}). For CA76.11, a broad band is observed in this region centered at 1100 cm^{-1}, in close resemblance to Raman spectra for Na-aluminosilicate system (Seifert et al., 1982; Neuville and Mysen, 1996). As the Al_2O_3 content increases, the high-frequency envelope narrows to a single asymmetric maximum, which shifts to lower frequency and whose intensity increases. The high-frequency peak shifts rapidly to low frequencies with decreasing SiO_2 content, from 1150 to 900 cm^{-1} for CA76.11 and CA12.44, respectively. For CA50.25, the high-frequency region consists of an asymmetric band at 1000 cm^{-1} with a shoulder near 1080 cm^{-1}. We can note that the frequencies of the maxima in this region decrease more rapidly with alumina content than the peaks in the low-frequency region. Raman modes in this region are assigned to the asymmetric and symmetric stretching vibrations of the fully-polymerized tetrahedral network units. These bands are assigned to (Si,Al)-NBO and (Si,Al)-BO (BO denotes bridging oxygens) stretch bands (Mysen, 1988) or discreet bands due to Si(OAl)x units, where x is the number of AlO_4 tetrahedra connected to a SiO_4 tetrahedron (McMillan et al., 1982). The shift to longer wavelengths has been attributed to a reduction in force constant (Seifert et al., 1982; Mysen et al., 1985), (Al,Si) coupling (Mysen et al., 1985) or to the superposition of Si(OAl)x units (McMillan and Piriou, 1982), reflecting substitution of Al^{3+} for Si^{4+}.

3.1.1.4. Spectral deconvolution. The high frequency region has been deconvoluted along the lines suggested previously (Seifert et al., 1982; Neuville and Mysen, 1996). Three gaussian bands were used for all compositions, near 1050, 1150 and 1200 cm^{-1}. Increasing the number of gaussian bands does not significantly affect the fit, the uncertainty being similar for three or four gaussian bands (Mysen, 1990, 1995).

3.1.2. Peraluminous Glasses

For all glasses with excess aluminum, the noise/intensity ratio increases by nearly an order of magnitude with alumina content. The bands become also wider and shift to high frequency.

3.1.2.1. Low-frequency region (200–700 cm^{-1}). Modifications of the Raman spectra appear for the band at 500 cm^{-1} with increasing aluminum content. The position of this peak is shifted towards higher frequency in the spectra and become wider for CA76.17. For glasses with 50 mol% of SiO_2 (CA50.25, CA50.30 and CA50.35), the two peaks at 500 and 550 cm^{-1} become broader with excess aluminum. Similar behavior was observed for CA33.38, CA33.43 and CA10.55 compare to CA33.33 and CA12.44, respectively. With excess aluminum, the width of the low frequency envelope increases by a factor of two. The shift in intensity and the broadening of the bands is more important in the Al_2O_3-rich glasses.

3.1.2.2. Midfrequency region (700–900 cm^{-1}). The intensity of the band at 800 cm^{-1} increases with adding aluminum in CA76.11. This band becomes wider and decreases in frequency. For glasses with less silica content (CA50.25, CA50.30, CA50.35), this band increases again in width and disappears for glasses with less than 50 mol % of silica.

3.1.2.3. High-frequency region (900–1300 cm^{-1}). The high frequency part of the CA76.17 shifts to high frequency compare with CA76.11. The Raman spectrum of CA76.11 exhibits a new broad band at 1100 cm^{-1}. Similar behavior was observed for the CA50.30 and CA50.35 compare to CA50.25. For glasses with less than 50 mol % of silica, we observe an increase of width and a broadening of the high frequency envelope.

3.2. XANES Spectroscopy

Normalized XANES spectra at the Al K-edge are presented in Figure 3 for all glasses. Two peaks labeled *a* and *b* are visible near the edge with variable relative intensities as a function of the chemical composition. In addition, there is a broad feature at ~1581 eV. The peak *a* corresponds to a 1s → 3p transition (Li et al., 1995) and its energy position has been previously used to quantify the $^{[4]}Al/^{[6]}Al$ ratio (Li et al., 1995; Andrault et al., 1998; Ildefonse et al., 1994). For glasses with $R = CaO/Al_2O_3 = 1$, peak *a* is located at 1565 eV and can be attributed to Al in four-fold coordination as for other CAS glasses with $CaO/Al_2O_3 \geq 1$ (Neuville et al., 2004). Peak *a* is the main resonance at high SiO_2 content but its intensity decreases with the addition of Al_2O_3 and, simultaneously, the intensity of peak *b* has grown so that both peaks have similar intensity for CA12.44.

For the peraluminous glasses, similar changes of the intensities of peak *a* and *b* are observed from the SiO_2-rich to the SiO_2-poor glasses. At constant SiO_2 content, the position of the resonance *a* shifts towards higher energy (+0.5 eV), especially for the CA33.43 and CA10.55 glasses. This effect can be attributed to the presence of a small amount (few %) of Al in five or sixfold coordination that exhibit a resonance *a* at higher energy than for the four fold coordinated cation (Ildefonse et al., 1994; Li et al., 1995; Andrault et al., 1998). In contrast, the position of peaks *a* is not significantly affected by the addition of Al_2O_3 in silica-rich glasses (76 and 50 mol% SiO_2). Addition of Al_2O_3 yields an intensity increase of peak *b* in SiO_2-rich glasses (76 and 50 mol% SiO_2) and an intensity increase of peak *a* in Al_2O_3-rich glasses (33 and 10 mol% SiO_2).

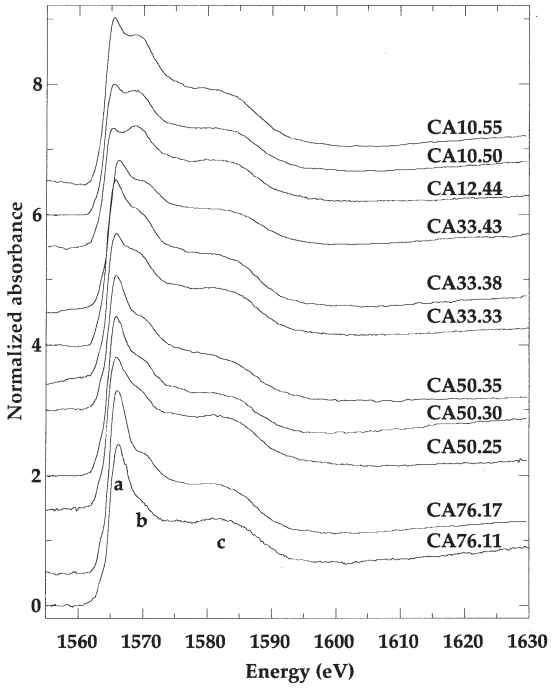

Fig. 3. XANES spectra at the Al k-edge for tectosilicate and peraluminous glasses.

3.3. NMR Spectroscopy

In MQMAS experiments, the intensity of the ^{27}Al resonance lines is spread in two dimensions according to their isotropic chemical shifts, quadrupolar couplings, and the distributions of these parameters. The chemical shift interaction effects are proportional to the principal field (B_0) when expressed in Hz or constant when expressed in ppm, which enables the direct comparison of spectra obtained at different fields. On the contrary, the second order quadrupolar interaction effects are proportional to the inverse of B_0 when expressed in Hz units (proportional to the inverse of B_0^2 when expressed in ppm). Consequently, the spectrum of a given sample shows very strong principal field dependence (Gan et al., 2002). The low field spectra (9.4 T—400 MHz) are dominated by second order quadrupolar shifts and broadening, while the high field spectra (17.6 T—750 MHz) exhibit higher resolution with reduced second order quadrupolar and enhanced chemical shift distribution effects.

Figure 4 shows the examples of spectra acquired for two glass samples (CA50.35 and CA50.30) at 400 and 750 MHz. The CA50.30 and CA50.25 glasses clearly show two overlapping contributions assigned to AlO_4 (higher chemical shift) and AlO_5 (lower chemical shift) (MacKenzie and Smith, 2002).

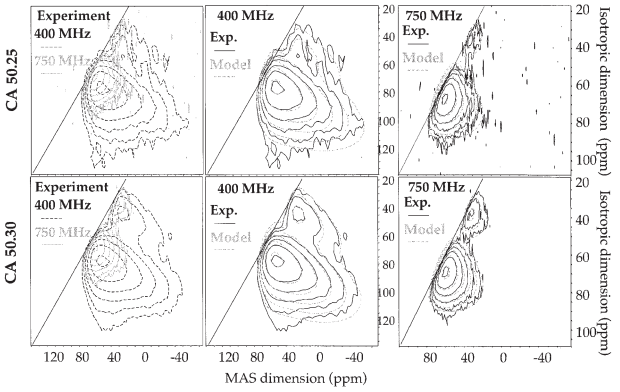

Fig. 4. ^{27}Al 3QMAS NMR spectra for the CA50.25 and CA50.30 glasses obtained at two different principal fields (9.4 T—400 MHz and 17.6 T—750 MHz). Comparison between the experimental spectra and the fitting model obtained with the same set of parameters for the two fields as explained in the text (lower contour levels are used for CA50.25 to make the AlO_5 contribution visible).

The CA50.25 shows a dominant AlO_4 signature with a small contribution of AlO_5, as already reported in the literature (Stebbins et al., 2000). A proper modeling or fitting of the spectra should be able to account for both the high and low field contrasted spectra with the same set of NMR parameters: isotropic chemical shift (δ_{iso}), quadrupolar interaction parameters (quadrupolar coupling ν_Q and asymmetry η_Q, or quadrupolar product $\nu_Q^* = \nu_Q \sqrt{1 + \eta_Q^2/3}$); and their distributions.

There exist several possibilities to account for the distribution of NMR parameters in spectra of glasses. The inversion methods aim at solving the ill-posed problem of deriving a chemical shift and quadrupolar interaction distributions from the experimental data set without making any assumptions. This has been convincingly applied to aluminosilicate glasses (Angeli et al., 2000a,b; Lafuma, 2003), though this method faces numerous difficulties in finding a stable final solution. It has been recently shown that modeled spectra can be computed from ab initio quantum chemical computation on the base of molecular dynamics models of the glasses (Charpentier et al., 2004).

In this contribution, we attempt to simulate the obtained spectra with a physically relevant model that makes the simplest assumption on the nature of the disorder in the glass phase, translated into the NMR parameters. The main difficulties arise with the interplay of a gaussian distribution of isotropic chemical shift (usually accessed as the width of the individual line in the case of a non quadrupolar nucleus like ^{29}Si) and the distribution of quadrupolar coupling that arises for the electric field gradient at the site of the observed nucleus. In that sense, the NMR quadrupolar parameters are of same nature as the quadrupolar splitting observed in Mössbauer spectroscopy.

The question of the distribution of electric field gradient has been addressed in the past in the scope of modeling Mössbauer spectra of disordered solids (Czjzek et al., 1981; Le Caër and Brand, 1998) and further applied to model NMR spectra of quadrupolar nuclei (Bureau et al., 1999; Hoatson et al., 2002). The electric field gradient arises from the distribution of cationic and anionic charges around the observed nucleus. The simplest physically consistent model is the gaussian Isotropic Model (GIM) (Le Caër and Brand, 1998) in which the Electric Field Gradient (EFG) is assumed to correspond to a statistical disorder. Under this assumption we can compute the probability of a given ν_Q, η_Q pair (or quadrupolar product ν_Q^*) that completely characterizes the traceless EFG or quadrupolar tensor, depending on a single parameter which is related to the quadratic mean of the quadrupolar product. The GIM distribution function has been implemented in a laboratory developed software (Massiot et al., 2002), which allows fitting of the obtained spectra with isotropic chemical shift mean value, distribution, and mean quadrupolar product.

As the chemical shift distribution remains field independent (when expressed in ppm) while the second order quadrupolar shifts and broadenings are proportional to $1/B_0^2$, the experiments at the two different fields provide very different spectra that should be accounted for by the same set of parameters if the model is valid. To validate the proposed model we can consider the typical case of CA50.30 and CA50.25. Table 2 (Fig. 4) reports the parameters obtained by fitting the ^{27}Al MQMAS at two very different principal fields (9.4 T—400 MHz and 17.6 T—750 MHz). For the two glasses the parameters obtained at the two fields are in very good agreement: isotropic chemical shift (δ_{iso}), distribution of chemical shift (d_{CSA}), and mean quadrupolar product (ν_Q^*). These parameters can be optimized to fit the best the 1D 750 MHz MAS spectra presented in Figure 5 for these two glasses. This model takes consistently into account central transition and spinning sidebands of the outer transitions. The obtained fit (Table 2) is good enough to suggest the presence of a low amount of AlO_6 environment (<2%) in the case of CA50.30, which remains hardly visible in the MQMAS spectrum. For 1D spectra acquired using small pulse angle, the proportions of the different species are computed from the integrated intensities of the central transition signatures (discarding the outer transitions in the 1D) (Massiot et al., 1990). In the case of MQMAS spectra, the integrated intensity of the different line also depends upon the quadrupolar product which drives the efficiency of the triple quantum coherence generation and transfer. In our case the quadrupolar product appear to be of the same order for all the different sites and integrated intensities do not have to be corrected for this effect.

The MQMAS spectra of the other samples (only obtained at 9.4 T—400 MHz) have then been fitted with the same assumptions (Fig. 6 and Table 2). For all spectra we observe a very satisfactory modeling especially when considering the simplicity of the model that accounts for the distribution of the quadrupolar coupling.

For our three samples along the compensation line ($CaO/Al_2O_3 = 1$), we observe the following trends:

- The mean isotropic chemical shift (δ_{iso}) of the AlO_4 signature increases linearly with alumina content along the compensation line (66, 71.5, 77.9 ppm) (Insert in Fig. 7). This trend is accompanied with a small but significant decrease of the width of the distribution of the chemical shift (dCSA) at the highest aluminum content (10 ppm instead of 13.5 for the two other samples).
- The mean isotropic chemical shift (δ_{iso}) of the AlO_4 contribution remains unchanged when going to peraluminous compositions (at a given SiO_2). The increased excess of Al only

Table 2. NMR parameters obtained by fitting the ^{27}Al MQ-MAS spectra.

	AlO_4				AlO_5			
Sample	Intens. (%)	δ_{iso} (ppm)	dCSA (ppm)	ν_Q* (kHz)	Intens. (%)	δ_{iso} (ppm)	dCSA (ppm)	ν_Q* (kHz)
CA50.25	93	66.0	13	1002	7	37.8	13	1148
CA50.25[b]	93	65.1	13	1084	7	34.9	13	883
CA50.25[c]	92	64.8	13	1080	8	38	13	1300
CA50.30	83	66.2	13	1064	17	35.7	15	1063
CA50.30[b]	84	65.2	14	1157	16	35.7	14	1003
CA50.30[c]	84	65.6	14	1270	14	36.4	14	1230
CA50.35	72	64.7	13	1026	28	35.2	18	1124
CA33.33	92	71.6	13	1033	8	38.4	21	1081
CA33.43	77	70.1	14	1090	23	38.0	16	1019
CA12.44	95	77.9	10	992	5	44.2	10	800
CA10.55	86	76.5	11	1051	14	42.1	13	1009

[a] δ_{iso} is the isotropic chemical shift, dCSA is the width of the gaussian distribution of δ_{iso}, ν_Q* is the quadrupolar product.
[b] Results obtained by fitting the high field MQMAS spectra of CA50.25 and CA50.30 at 750 MHz.
[c] Results obtained by fitting the 1D MAS spectra of CA50.25 and CA50.30 at 750 MHz. The 1D MAS spectrum of CA50.30 evidences a minor but significant (<2%) signature of [6]A1 (δ_{iso} 14.5 ppm, ν_Q* 1380 kHz).

produces higher coordination Al species [5]Al (and minor amounts of [6]Al).

- The measured quadrupolar product (ν_Q*) remains nearly constant upon substitution of Si by Al as neighboring tetrahedral units.

4. DISCUSSION

The NMR results indicate the presence of five-fold coordinated Al species, [5]Al, in both tecto- and peraluminous glasses. A minor amount (less that 2%, Table 2) of sixfold coordination, [6]Al, has been detected in CA50.30 which is the only peraluminous composition obtained with the two different principal fields. The proportion of [5]Al has been quantitatively determined. For CA50.25 and CA50.30, the fits of experiments at two different fields, yielding very contrasted spectra, give similar results, for NMR parameters and for quantification, validating the fitting procedure. The parameters are reported in Table 2 and indicate that [5]Al is present along the joins CaO/Al_2O_3 at about the same concentration with addition of Al_2O_3. The previously reported proportion of [5]Al in anorthite glass was 1%–2% (Stebbins et al., 2000) but this value was an estimate and not derived from quantitative analysis as in the present study. This high coordinated units must be associated with NBOs which were revealed using ^{17}O 3QMAS NMR (Stebbins and Xu, 1997) with a proportion of ~5% of the oxygens as NBOs in anorthite (Ca50.25) glass. Our finding of ~7% [5]Al could explain the presence of NBOs without the recourse to O triclusters. Five-fold coordinated Al has been also observed in Mg tectosilicate glasses (Toplis et al., 2000) with a similar concentration and in a CA58.29 glass (Sato et al., 1991), in agreement with the present results.

In peraluminous glasses, the proportion of [5]Al increases as expected since not enough Ca is present to ensure charge compensation of AlO_4 tetrahedra. The highest proportion of [5]Al is found at 50 mol% SiO_2 (Ca50.35). Adding 10% of Al_2O_3 leads to the formation of more [5]Al at 50 mol% SiO_2 than at 12 mol% SiO_2. This trend could indicate that more O triclusters are formed at low silica content that is close to the

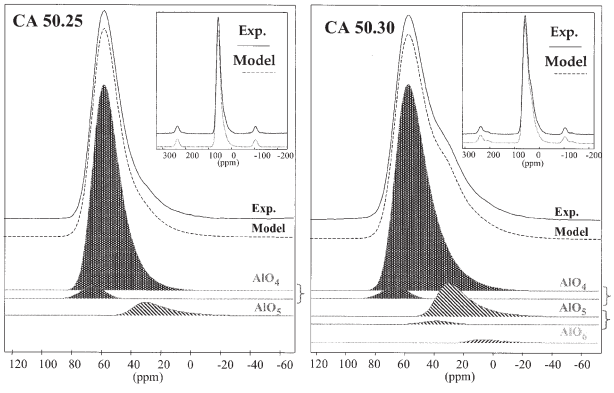

Fig. 5. ^{27}Al 1D MAS NMR spectra (750 MHz) of CA50.25 and CA50.30. The inserts show experimental and simulated spectra of central transition and first spinning sidebands of the outer transitions. The main figure shows the individual contribution of the different sites: AlO_4, AlO_5, and AlO_6, including the $n = 0$ spinning sideband of the satellite transitions when visible.

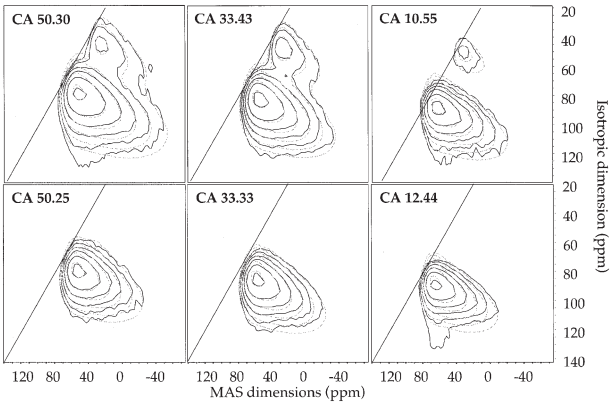

Fig. 6. ^{27}Al 3QMAS NMR spectra for different tecto- (bottom) and peraluminous (top) glasses comparing experiment (plain curves) and simulation (dashed curves). All figures are drawn with the same contour levels.

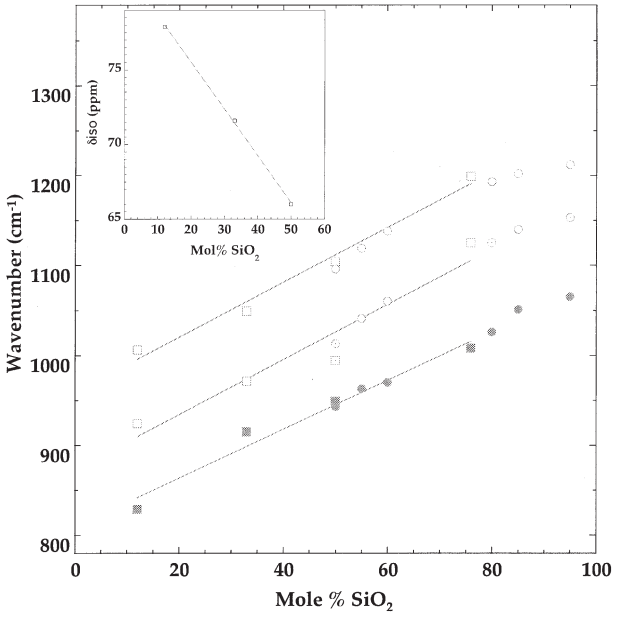

Fig. 7. Dependence of Raman frequencies of the 1050, 1150 and 1200 cm^{-1} bands upon the SiO_2 content. The circles are for the SiO_2-$NaAlO_2$ glasses (Neuville and Mysen, 1996) and the squares for the SiO_2-$CaAl_2O_4$ glasses. Insert. Similar dependence of δ_{iso} determined in the NMR fitting (Table 2) upon the SiO_2 content. Lines are only guides for the eye.

$CaAl_4O_7$ (Grossite) structure, which is the only crystal in this system that contains triclusters (Goodwin and Lindop, 1970). According to the bond valence model (O'Keefe, 1990; Brese and O'Keefe, 1991), it would be energetically more favorable for an O tricluster to be associated with two or three AlO_4 tetrahedra than with SiO_4 tetrahedra because the overbonding in the latter case will be smaller.

Modification of the Al coordination produces only a small change of the XANES spectra at Al K-edge, which is somewhat surprising considering the variations of this edge along the SiO_2-$CaAl_2O_4$ joins (Fig. 3). The modifications observed in the XANES spectra upon Si/Al substitution cannot be ascribed to change of atomic weight between Si and Al and must thus have a structural origin. For tectosilicate compositions, Al should be mainly in Q^4 position because few NBOs exist in such compositions. Hence, the variations of intensity of peaks *a* and *b* cannot be related to network polymerization as in other CAS glasses (Neuville et al., 2004). Instead, variations of Al-(Si,Al) bond lengths and Al-O-(Si,Al) intertetrahedral angles has been proposed to explained these modifications (Wu et al., 1999). This is in consistent with our MD models (Cormier et al., 2003) in which we observe an increase of the average intertrahedral angle with increasing silica content. The variation of the intertrahedral angle is associated with the formation of larger membered rings in SiO_2-rich glasses (typically 5-membered rings) while 4-membered rings prevail at low-silica content. A similar explanation holds for other joins as silica is added but network repolymerization must also be taken into account (Neuville et al., 2004). Further theoretical calculations are required to fully understand and interpret the chemical dependence of Al K-edge XANES spectra (Cabaret et al., 1996). In peraluminous glasses, slight variations in the position of the edge and in the relative intensities of peaks *a* and *b* are observed but a quantitative determination of high coordinated Al sites is difficult. The reason could be the small difference in the XANES spectra of $^{[4]}$Al and $^{[5]}$Al in disordered materials.

In the Raman spectra of glasses along the join SiO_2-$CaAl_2O_4$, we observe a continuous shift of the band frequencies towards higher wave numbers as a function of increasing SiO_2 (Fig. 7). It is interesting to remark that, similarly, the three measurements of δ_{iso} for $^{[4]}$Al in tectosilicate glass compositions give a linear decreasing relation as a function of increasing SiO_2 (inset in Fig. 7) Band frequencies and δ_{iso} are thus reflecting the Si/Al substitution in the second neighbor shell of AlO_4 tetrahedra. There is no evidence of new bands forming as composition is changed along the tectosilicate join. These observations are consistent with continuous substitution of Ca^{2+}-charge-balanced Al^{3+} for Si^{4+} in tetrahedral coordination in the two structural units for all compositions. These results are in good agreement with those observed by Seifert et al. (1982) and Neuville and Mysen (1996). In Figure 7, we have also plotted the variations in frequencies for the SiO_2-$NaAlO_2$ glasses (Neuville and Mysen, 1996). We observed a very good agreement for these two sets of data and the frequencies for the CaO or Na_2O system appear to be the same for these three bands.

The Raman bands corresponding to $^{[5]}$Al or $^{[6]}$Al are expected to occur at low frequency and to be weak. The detection of such species should thus be difficult. However, such coordination transformation is associated with the formation of NBOs which could give Raman bands (Mysen et al., 1985). Mysen and Virgo (1980) suggested that bands at 950 and 1100 cm^{-1} appearing along the SiO_2-Al_2O_3 join are due to NBOs. In our Raman spectra, such bands do not clearly appear for the glasses containing the higher concentration of cAl. On the contrary, they appear at high SiO_2 content. McMillan and Piriou (1982) suggested that they are due to stretching vibrations of SiO_4 tetrahedra bound to one and two Al atoms for the 1100 and 950 cm^{-1} bands, respectively. A compression study of $CaAl_2O_4$ indicates a broad Raman band at 750 cm^{-1} appearing at high pressure, which was ascribed to highly coordinated Al sites ($^{[5]}$Al and/or $^{[6]}$Al) with simultaneous formation of triclusters (Daniel et al., 1996). From infrared studies, the region 680–400 cm^{-1} was ascribed to stretching modes of AlO_6 octahedra (Tarte, 1964; Poe et al., 1992). In the Raman spectra, peaks near 580 cm^{-1} and 700 cm^{-1} grow in intensity and a shoulder appears at 450 cm^{-1} with the addition of Al_2O_3 in peraluminous glasses and these bands could correspond to the $^{[5]}$Al sites.

The lack of important content of $^{[6]}$Al is consistent with the early prediction of Lacy (1963) that rejected this possibility on the basis of packing arguments. However, the existence of $^{[6]}$Al has been detected in CAS glasses near the SiO_2-Al_2O_3 join (Sato et al., 1991; Poe et al., 1992). The proportion of $^{[5]}$Al quantified for the tectosilicate glass should have important effect on the physical and thermodynamic properties of the glasses and melts, such as transport and crystallization. It was proposed that $^{[5]}$Si present in alkali silicate species could serve as a transient units during the viscous flow (Farnan and Stebbins, 1994) and $^{[5]}$Al could thus have major influence in the transport mechanisms of glasses near tectosilicate compositions and explain variations in viscosity (Toplis et al., 1997b). The

number of [5]Al and [6]Al species should increase with temperature as inferred from MD simulation (Poe et al., 1992) and should be related to the thermal history of the glass. These high-coordinated Al species are thus believed to play an important role in Al_2O_3 rich glasses and melts and contribute to configurational thermodynamic properties.

5. CONCLUSIONS

From high resolution ^{27}Al NMR, using different high-field, and careful fitting of the NMR data, the local Al environment has been accurately determined in tecto- and peraluminous glasses in CaO-SiO_2-Al_2O_3 system. A significant proportion of [5]Al (7%) is present in tectosilicate and peraluminous glasses with only minor amount of [6]Al in the CA50.30 glass. The proportion of [5]Al is higher than previously determined which could indicate that O triclusters are less important that previously estimated to explain the variation in viscosity near the tectosilicate compositions. Though the XANES spectra are strongly dependent upon the Si/Al substitution along a join at constant CaO/Al_2O_3 ratio, the variations of the XANES spectra with the proportion of [5]Al is much less important. Raman spectra have been deconvoluted at high frequencies, in a region showing a strong dependence with the $CaAl_2O_4$ content. The band frequencies vary with SiO_2 in a similar manner than for Na_2O-SiO_2-Al_2O_3 glasses, and are inversely correlated with the variations of the NMR isotropic chemical shift (δ_{iso}). These similar linear variations could indicate that the δ_{iso} and the Raman band frequencies are sensible to the same units in silicate liquid. Characteristic bands of [5]Al or [6]Al are difficult to determine in the Raman spectra showing that this technique is not sensitive enough to such species. The presence of highly coordinated Al species should be of great importance at high temperature and pressure and must be taken into account to understand physical and thermodynamical properties of glasses and melts.

Acknowledgments—We thank J. C. Rifflet and F. Millot (CRMHT-CNRS) for their help during the peraluminous glass preparation; A-M. Flank and P. Lagarde during the acquisition of the XANES data at LURE (Orsay); H. Forster, S. Steuernagel and Bruker Karlsruhe for acquisition of 750 MHz spectra; Région Centre for financial support; G. Calas and P. Richet for useful discussions. We gratefully acknowledge thoughtful comments by J. Stebbins and B. Mysen. This is IPGP contribution N°1987.

Associate editor: B. Mysen

REFERENCES

Alemany L. B., Massiot D., Sherrif B. L., Smith M. E., and Taulelle F. (1991) Observation and accurate quantification of Al-27 MAS NMR spectra of some Al_2SiO_5 polymorphs containing sites with large quadrupole interactions. *Chem. Phys. Lett.* **177,** 301–306.

Allwardt J. R., Lee S. K., and Stebbins J. F. (2003) Bonding preferences of non-bridging O atoms: Evidence from ^{17}O MAS and 3QMAS NMR on calcium aluminate and low-silica Ca-aluminosilicate glasses. *Am. Min.* **88,** 949–954.

Andrault D., Neuville D. R., Flank A.-M., and Wang Y. (1998) Cation sites in Al-rich $MgSiO_3$ perovskites. *Am. Min.* **83,** 1045–1053.

Angeli F., Delaye J. M., Charpentier T., Petit J. C., Ghaleb D., and Faucon P. (2000a) Influence of glass chemical composition on the Na-O bon distance: A ^{23}Na 3Q-MAS NMR and molecular dynamic study. *J. Non-Cryst. Solids* **276,** 132–144.

Angeli F., Delaye J. M., Charpentier T., Petit J. C., Ghaleb D., and Faucon P. (2000b) Investigation of Al-O-Si bond angle in glass by ^{27}Al 3Q-MAS NMR and molecular dynamics *Chem. J. Phys. Lett.* **320,** 681–687.

Benoit M., Ispas S., and Tuckerman M. E. (2001) Structural properties of molten silicates from ab initio molecular-dynamics simulations: Comparison between CaO-Al_2O_3-SiO_2 and SiO_2. *Phys. Rev. B* **64,** 224205-1–224205-10.

Brese N. E. and O'Keefe M. (1991) Bond-valence parameters for solids. *Acta Cryst. B* **47,** 192–197.

Bureau B., Silly G., Buzaré J. Y., Legein C., and Massiot D. (1999) From crystalline to glassy gallium fluoride materials: An NMR study of ^{69}Ga and ^{71}Ga quadrupolar nuclei. *Sol. State NMR* **14,** 191–202.

Cabaret D., Sainctavit, Ph., Ildefonse Ph., Calas G., and Flanck A.-M. (1996) Full multiple scattering calculations at Al K-edge on alumino-silicates and Al-oxides. *Phys. Chem. Min.* **23,** 226–229.

Charpentier T., Ispas S., Profeta M., and Mauri F. (2004) First principles calculations of ^{17}O, ^{29}Si and ^{23}Na NMR spectra of sodium silicate crystals and glasses. *J. Phys. Chem. B*, **108,** 4147–4167.

Cormier L., Neuville D. R., and Calas G. (2000) Structure and properties of low-silica calcium aluminosilicate glasses. *J. Non-Cryst. Solids* **274,** 110–114.

Cormier L., Ghaleb D., Neuville D. R., Delaye J.-M., and Calas G. (2003) Chemical dependence of network topology of calcium aluminosilicate glasses: A molecular dynamics and reverse Monte Carlo study. *J. Non-Cryst. Solids* **332,** 255–270.

Cormier L., Neuville D. R., and Calas G. (2004) Relationship between structure and glass transition temperature in low-silica calcium aluminosilicate glasses: The origin of the anomaly at low silica content. *J. Am. Ceram. Soc.,* in press.

Coté B., Massiot D., Taulelle F., and Coutures J.-P. (1992) ^{27}Al NMR spectroscopy of aluminosilicate melts and glasses. *Chem. Geol.* **96,** 367–370.

Czjzek G., Fink J., Götz F., Schmidt H. Coey J. M. D., Rebouillat J. P., and Liénard A. (1981) Atomic coordination and the distribution of electric field gradients in amorphous solids. *Phys. Rev B* **23,** 2513–2530.

Daniel I., McMillan P. F., Gillet P., and Poe B. T. (1996) Raman spectroscopic study of structural changes in calcium aluminate ($CaAl_2O_4$) glass at high pressure and high temperature. *Chem. Geol.* **128,** 5–16.

Farnan I. and Stebbins J. F. (1994) The nature of the glass transition in a silica-rich oxide melt. *Science* **265,** 1206–1208.

Frydman L. (2002) Fundamentals of multiple-quantum magic-angle spinning NMR on half-integer quadrupolar nuclei. In *Encyclopedia of Nuclear Magnetic Resonance.* Vol. 9 Wiley.

Frydman L. and Harwood J. S. (1995) Isotropic spectra of half-integer quadrupolar spins from bidimensional magic-angle spinning. *J. Am. Chem. Soc.* **117,** 5367–5368.

Gan Z., Gor'kov P., Cross T. A., Samoson A., and Massiot D. (2002) Seeking higher resolution and sensitivity for NMR of quadrupolar nuclei at ultrahigh magnetic fields. *J. Am. Chem. Soc.* **124,** 5634–5635.

Goodwin D. W. and Lindop A. J. (1970) The crystal structure of $CaO \cdot 2Al_2O_3$. *Acta Cryst. B* **26,** 1230–1235.

Hoatson G. L., Zhou D. H., Fayon F., Massiot D., and Vold R. L. (2002) 93Nb magic angle spinning NMR study of perovskite relaxor ferroelectrics. (1−x)Pb(Mg1/3Nb2/3)O3-xPb(Sc1/2Nb1/2)O3. *Phys. Rev. B* **66,** 224103–1–13.

Ildefonse P., Kirkpatrick R. J., Montez B., Calas G., Flank A.-M., and Lagarde P. (1994) ^{27}Al MAS NMR and aluminium X-ray absorption near edge structure study of imogolite and allophanes. *Clays and Clay Minerals* **42** (*3*), 276–287.

Lacy E. D. (1963) Aluminium in glasses and melts. *Phys. Chem. Glasses* **4,** 234–238.

Lafuma L., Fayon F., Massiot D., Chodorowski Kimmes S., and Sanchez C. (2003) Solid-state NMR characterization of oxygen sites in organically modified aluminosilicate xerogels. *Magn. Res. Chem.* **41,** 944–948.

Le Caër G. and Brand R. A. (1998) General models for the distributions of electric field gradients in disordered solids. *J. Phys. Condens. Matter* **10,** 10715–10774.

Li D., Bancroft G. M., Fleet M. E., Feng X. H., and Pan Y. (1995) Al K-edge XANES spectra of aluminosilicate minerals. *Am. Min.* **80,** 432–440.

Lines M. E., MacChesney J. B., Lyons K. B., Bruce A. J., Miller A. E., and Nassau K. (1989) Calcium aluminate glasses as pontential ultralow-loss optical materials at 1.5–1.9 μm. *J. Non-Cryst. Solids* **107,** 251–260.

Long D. A. (1977) *Raman Spectroscopy.* McGraw-Hill.

MacKenzie K. J. D. and Smith M. E. (2002) *Multinuclear Solid State NMR of Inorganic Materials*. Pergamon.

Massiot D. (1996) Sensitivity and lineshape improvements of MQ-MAS by rotor synchronized data acquisition. *J. Mag. Reson. A* **122,** 240–244.

Massiot D., Bessada C., Coutures J. P., and Taulelle F. (1990) A quantitative study of aluminum-27 MAS NMR in crystalline YAG. *J. Magn. Reson.* **90,** 231–242.

Massiot D., Touzo B., Trumeau D., Coutures J. P., Virlet J., Florian P., and Grandinetti P. J. (1996) Two-dimensiontal magic-angle spinning isotropic reconstruction sequences for quadrupolar nuclei. *Sol. State NMR* **6,** 73–83.

Massiot D., Fayon F., Capron M., King I., Le Calvé S., Alonso B., Durand, J-O., Bujoli B., Gan Z., and Hoatson G. (2002) Modelling one and two-dimensional solid-state NMR spectra. *Mag. Res. Chem.* **40,** 70–76.

McMillan P. and Piriou B. (1982) The structures and vibrational spectra of crystals and glasses in the silica-alumina system. *J. Non-Cryst. Solids* **53,** 279–298.

McMillan P., Piriou B., and Navrotsky A. (1982) A Raman spectroscopic study of glasses along the joins silica-calcium aluminate, silica-sodium aluminate and silica-potassium aluminate. *Geochim. Cosmochim. Acta* **46,** 2021–2037.

McMillan P. F., Poe B. T., Gillet Ph., and Reynard B. (1994) A study of SiO_2 glass and supercooled liquid to 1950 K via high-temperature Raman spectroscopy. *Geochim. Cosmochim. Acta* **58,** 3653–3664.

Medek A., Harwood J. S., and Frydman L. (1995) Multiple-quantum magic-angle spinning NMR: A new method for the study of quadrupolar nuclei in solids. *J. Am. Chem. Soc.* **117,** 12779–12787.

Mysen B. O. (1988) *Structure and Properties of Silicate Melts.* Elsevier.

Mysen B. O. (1990) Effect of pressure, temperature and bulk composition on the structure and species distribution in depolymerized alkali aluminosilicate melts and quenched melts. *J. Geophys. Res.* **95,** 15733–15744.

Mysen B. O. (1995) Structural behavior of Al^{3+} in silicate melts: In situ, high-temperature measurements as a function of bulk chemical composition. *Geochim. Comoschim. Acta* **59,** 455–474.

Mysen B. O. and Virgo D. (1980) Trace element partitioning and melt structure: An experimental study at 1 atm.pressure. *Geochim. Cosmochim. Acta* **44,** 1917–1930.

Mysen B. O., Virgo D., and Kushiro I. (1981) The structural role of aluminium in silicate melts—A Raman spectroscopic study at 1 atmosphere. *Am. Min.* **66,** 678–701.

Mysen B. O., Virgo D., and Seifert F. A. (1985) Relationships between properties and structure of aluminosilicate melts. *Am. Min.* **70,** 88–105.

Neuville D. R. (1992) Etudes des propriétés thermodynamiques et rhéologiques des silicates fondus. Ph.D. thesis. Université Paris VII.

Neuville D. R. and Mysen B. O. (1996) Role of aluminium in the silicate network: In situ, high-temperature study of glasses and melts on the join SiO_2-$NaAlO_2$. *Geochim. Comoschim. Acta* **66,** 1727–1737.

Neuville D. R., Cormier L., Boizot B., and Flank A.-M. (2003) Structure of β-irradiated glasses studied by X-ray absorption and Raman spectroscopies. *J. Non-Cryst. Solids* **323,** 207–213.

Neuville D. R., Cormier L., Flank A.-M., Briois V., and Massiot D. (2004) Al speciation and Ca environment in calcium aluminosilicate glasses and crystals by Al and Ca K-edge X-ray absorption spectroscopy. *Chem. Geol.,* in press.

O'Keefe M. (1990) A method for calculating bond valences in crystals. *Acta Cryst. A* **46,** 138–142.

Poe B. T., McMillan P. F., Angell C. A., and Stao R. K. (1992) Al and Si coordination in SiO_2-Al_2O_3 glasses and liquids: A study by NMR and IR spectroscopy and MD simulations. *Chem. Geol.* **96,** 333–349.

Sato R. K., McMillan P. F., Dennison P., and Dupree R. (1991) A structural investigation of high-alumina glasses in the CaO-Al_2O_3-SiO_2 system via Raman and magic angle spinning nuclear magnetic resonance spectroscopy. *Phys. Chem. Glasses* **32** (*4*), 149–156.

Seifert F., Mysen B. O., and Virgo D. (1982) Three-dimensional network structure of quenched melts (glass) in the system SiO_2-$NaAlO_2$, SiO_2-$CaAl_2O_4$ and SiO_2-$MgAl_2O_4$. *Am. Min.* **67,** 696–717.

Stebbins J. and Xu Z. (1997) NMR evidence for excess non-bridging oxygens in an aluminosilicate glass. *Nature* **390,** 60–62.

Stebbins J. F., Kroeker S., Lee S. K., and Kiczenski T. J. (2000) Quantification of five- and six-coordinated aluminium ions in aluminosilicate and fluoride-containing glasses by high-field, high-resolution ^{27}Al NMR. *J. Non-Cryst. Solids* **275,** 1–6.

Tarte P. (1964) Infra-red spectra of inorganic aluminates and characteristic vibrational frequencies of AlO_4 tetrahedra and AlO_6 octahedra. *Spectrochim. Acta* **23A,** 2127–2143.

Taylor M. and Brown G. E. Jr. (1979), Structure of mineral glasses—I. The feldspar glasses $NaAlSi_3O_8$, $KAlSi_3O_8$, $CaAl_2Si_2O_8$. *Geochim. Cosmochim. Acta* **43** 61–75.

Toplis M. J., Dingwell D. B., and Lenci T. (1997a) Peraluminous viscosity maxima in Na_2O-Al_2O_3-SiO_2 liquids: The role of triclusters in tectosilicate melts. *Geochim. Cosmochim. Acta* **61,** (*13*), 2605–2612.

Toplis M. J., Dingwell D. B., Hess K.-U., and Lenci T. (1997b) Viscosity, fragility and configurational entropy of melts along the join SiO_2-$NaAlSiO_4$. *Am. Min.* **82,** 970–990.

Toplis M. J., Kohn S. C., Smith M. E., and Poplett I. J. F. (2000) Fivefold-coordinated aluminium in tectosilicate glasses observed by triple quantum MAS NMR. *Am. Min.* **85,** 1556–1560.

Winterer M. (1997) XAFS—A data analysis program for materials science. *J. Phys. IV* **7** (C2), 243–244.

Wallenberger F. T. and Brown S. D. (1994) High-modulus glass fibers for new transportation and infrastructure composites and new infrared uses. *Comp. Sci. Tech.* **51,** 243–263.

Wu Z., Romano C., Marcelli A., Mottana A., Cibin G., Della Ventura G., and Giuli G. (1999) Evidence for Al/Si tetrahedral network in aluminosilicate glasses from Al K-edge X-ray–absorption spectroscopy. *Phys. Rev. B* **60** (*13*), 9216–9219.